Virginia Commonwealth University
VCU Scholars Compass

Chemistry Publications

Dept. of Chemistry

2008

Magnetic properties of La 0.6 Sr 0.4 MnO 3 thin films on SrTiO 3 and buffered Si substrates with varying thickness

A. K. Pradhan
Norfolk State University

D. Hunter
Norfolk State University

T. Williams
Norfolk State University

See next page for additional authors

Follow this and additional works at: http://scholarscompass.vcu.edu/chem_pubs

Part of the Chemistry Commons

Pradhan, A. K., Hunter, D., & Williams, T., et al. Magnetic properties of La(0.6)Sr(0.4)MnO(3) thin films on SrTiO(3) and buffered Si substrates with varying thickness. Journal of Applied Physics, 103, 023914 (2008). Copyright © 2008 American Institute of Physics.

Downloaded from

http://scholarscompass.vcu.edu/chem_pubs/21

Authors

A. K. Pradhan, D. Hunter, T. Williams, B. Lasley-Hunter, R. Bah, H. Mustafa, R. Rakhimov, J. Zhang, D. J. Sellmyer, E. E. Carpenter, D. R. Sahu, and J. -L. Huang

Magnetic properties of La$_{0.6}$Sr$_{0.4}$MnO$_3$ thin films on SrTiO$_3$ and buffered Si substrates with varying thickness

A. K. Pradhan,[1,a)] D. Hunter,[1] T. Williams,[1] B. Lasley-Hunter,[1] R. Bah,[1] H. Mustafa,[1] R. Rakhimov,[1] J. Zhang,[2] D. J. Sellmyer,[2] E. E. Carpenter,[3] D. R. Sahu,[4] and J.-L. Huang[4]

[1]*Center for Materials Research, Norfolk State University, 700 Park Avenue, Norfolk, Virginia 23504, USA*
[2]*Department of Physics and Astronomy and Center for Materials Research and Analysis, University of Nebraska, Lincoln, Nebraska 68588-0113, USA*
[3]*Virginia Commonwealth University, 1001 W. Main Street, P.O. Box 842006, Richmond, Virginia 23284-2006, USA*
[4]*Department of Materials Science & Engineering, National Cheng Kung University, Tainan 701, Taiwan*

La$_{0.60}$Sr$_{0.40}$MnO$_3$ (LSMO) thin films of varying thickness from 12 to 55 nm were deposited using the pulsed-laser deposition technique onto single-crystalline SrTiO$_3$ (STO) and STO-buffered Si substrates. The T_c of LSMO films grown on STO-buffered Si substrates decreases faster than films directly grown on STO with decreasing film thickness. The LSMO/STO film with thickness of 55 nm shows T_c at about 360 K, which is close to the bulk value, whereas T_c LSMO film on STO-buffered Si film of similar thickness is reduced to 320 K. This difference is attributed to the strain and interfacial disorders in LSMO film on STO/Si. The film surface morphology is influenced by the film thickness. Oxygenation of LSMO films on STO-buffered Si affects the T_c minimally but improved the overall magnetization of the films due to better oxygenation, which is also the case for postannealing the sample at elevated temperatures. The thermomagnetic history effects observed in LSMO films of STO-buffered Si indicate the presence of inhomogeneity, mostly at the interface, which influences the magnetic properties significantly. © *2008 American Institute of Physics*. [DOI: 10.1063/1.2833388]

I. INTRODUCTION

Doped perovskite manganites that show ferromagnetism above room temperate[1] have received a great deal of interest because of their potential use for various device applications such as infrared detectors, magnetic field sensors,[2,3] and high-density memory applications. In recent years, manganite films such as (La$_{1-x}$Sr$_x$)MnO$_3$ (LSMO) have stimulated intense study due to their colossal magnetoresistance (CMR) effect[4,5] and spin-dependent tunneling, which makes them attractive candidates for high-performance magnetic devices. In particular, integrating LSMO onto Si, the essential material of the semiconductor industry, is crucial in maximizing their potential use. Among most of the electrofunctional perovskite oxides, the characteristics of manganite compounds are very sensitive to lattice distortion imposed by chemical substitution or hydrostatic pressure. In the case of epitaxial heterostructures, a biaxial strain is induced at the interface if the lattice constant is different and the arrangement of atoms is coherent to that of the substrate. On the other hand, the strain relaxation of lattice mismatch between the film and the substrate at the interfaces occurs as the film thickness increases beyond a certain critical thickness of the film.[6]

The film grows coherently, storing the biaxial strain energy below a critical thickness (t_c). Above t_c, the elastic energy (due to the strain in the film, especially at the interface) in the strained film exceeds that in the core of misfit dislocation which would be introduced at the film–substrate interface. As a result, the film is relaxed to exhibit lattice constant similar to the bulk sample. Understanding and controlling the strain induced by lattice mismatching in perovskite manganites on their physical properties is crucial for realizing applications, because most applications demand ultrathin layers. The physics and the application of the doped manganites in magnetoresistive devices based on thin-film structures are affected by the strong dependence of their properties on strain[7–16] and their unknown interface properties. Although large effects due to volume preserving uniaxial strain are expected due to the relevance of the Jahn–Teller effect,[8] the detailed effect of strain on the electrical transport and magnetic properties of the CMR materials, as well as the magnetic properties at interfaces in the doped manganites, are not well understood so far. However, many proposed applications rely on thin-film structures where strain effects due to lattice mismatch between film and substrate in most cases cannot be avoided. Integrating the manganites onto the semiconducting materials such as Si remains a challenging task for potential device applications that utilize both information processing and data storage in the same device, and for designs of artificial structures intended to integrate with mainstream microelectronic devices based on growing perovskite oxide thin films on conventional semiconductors. However, there have been only a few reports on the fabrication and understanding of these artificially designed structures based on perovskite oxide thin films on silicon. In this paper, we

a)Also at Department of Engineering, Norfolk State University, 700 Park Avenue, Norfolk, Virginia 23504, USA. Electronic mail: apradhan@nsu.edu.

report the fabrication of ultrathin films of LSMO grown on single-crystalline $SrTiO_3$ (STO) and STO-buffered Si(100) substrates with varying thickness. We demonstrate that 55 nm thick films show transition temperatures close to those of bulk material. The reasons for the reduction of T_c with decreasing film thickness are illustrated, taking into account the strain effects due to pseudomorphic growth of the films.

II. EXPERIMENTAL

The $La_{0.6}Sr_{0.4}MnO_3$ thin films were grown by multitarget pulsed-laser deposition (PLD) technique (KrF excimer (λ =248 nm), with a pulse energy density of $1-2$ J/cm^2 and utilizing both target rotation and rastering, and substrate rotation facilities. Single-crystalline STO and high-density LSMO targets were used. LSMO calcined powders were isostatically pressed at 400 MPa and sintered at 1450 (C in order to make a high-density target). An STO substrate or an STO template layer on Si has been chosen because of its low (0.9%) lattice mismatch with LSMO which has the highest bulk T_c. The films were deposited on single-crystalline STO (100) and STO-buffered Si(100) substrates with a substrate temperature of $700-850$ °C, keeping oxygen partial pressure of 1–200 mTorr. The substrate was loaded to the chamber using a load-lock facility attached to the chamber and heated in the chamber at a rate of 20 °C/min just after the ultimate base pressure of $<3\times10^{-8}$ Torr to avoid the oxidation of the Si substrate before depositing STO, as described earlier.[17] The films were cooled at a cooling rate of 10 °C/min in O$_2$ of 500 Torr partial pressure from the growth temperature down to 300 °C, and then allowed to cool naturally to room temperature. The thickness of the film was precisely controlled by the number of pulses. The structural studies indicate that LSMO/STO films are highly epitaxial. Similarly, LSMO/STO/Si films are textured and oriented. The films were postannealed at 850 °C for 2 h with a heating and cooling rate of 10 °C/min.

Surface microstructure of the films was analyzed by atomic force microscopy (AFM). Magnetization (M) and magnetic hysteresis were measured by a superconducting quantum interference device (SQUID) magnetometer with in-plane magnetic field. Temperature dependence of electrical conductivity and current-voltage ($I-V$) characteristics were measured by a semiconductor parameter analyzer using In or In/Au contact pads.

III. RESULTS AND DISCUSSION

Two kinds of films, LSMO/STO and LSMO/STO/Si, of various thicknesses t_c (55 nm) were grown in order to compare their magnetic properties. The effects of film thickness on the surface morphology and magnetic properties of LSMO/STO films are discussed first. Figures 1(a) and 1(b) show the AFM images of LSMO/STO films with LSMO film thickness of 55 nm and 22 nm, respectively. It is very clear that the film is atomically smooth with a surface roughness of 0.7 nm. Large areas >0.5 μm with a surface roughness even less than 0.2 nm are seen. However, this decreases to about 80–100 nm area with increased surface roughness to 1.9 nm.
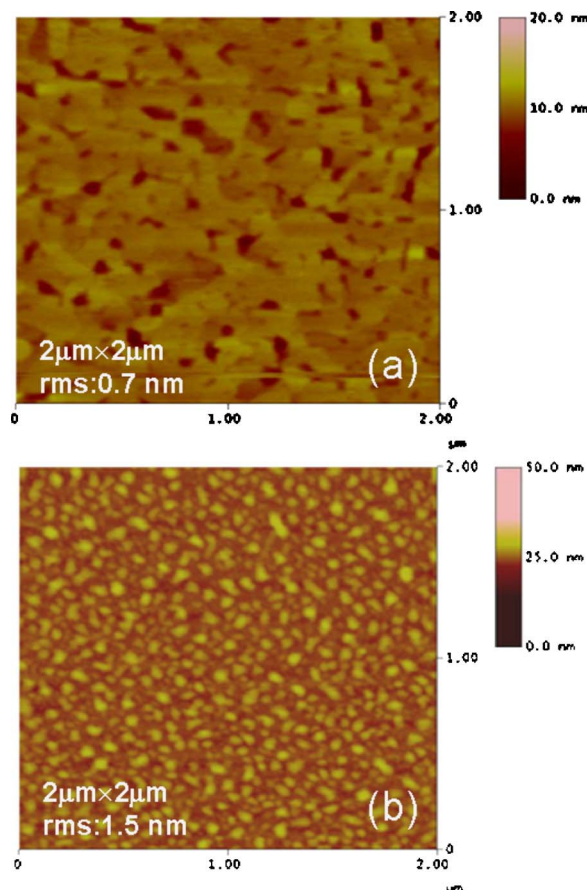

FIG. 1. (Color online) AFM images of (a) LSMO/STO of 55 nm and (b) 22 nm thick films.

Figure 2 demonstrates the temperature dependence of the field-cooled (FC) magnetization behavior of LSMO/STO films with varying thickness of LSMO films, such as 55, 22, and 12 nm. The magnetic field was applied parallel to the film surface in all films in the present work. The inset shows
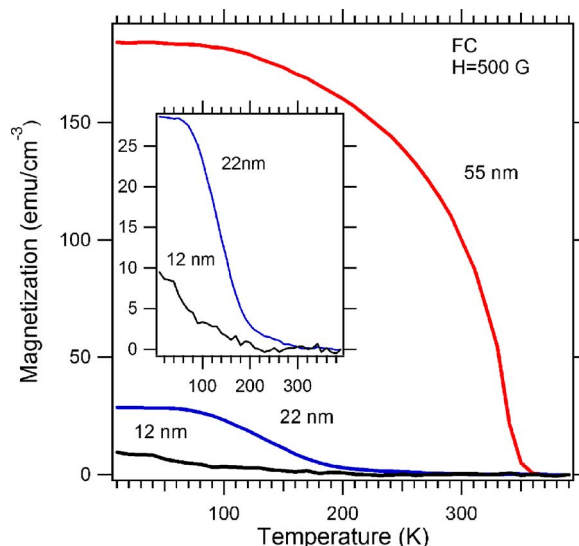

FIG. 2. (Color online) Temperature dependence of FC magnetization of LSMO/STO films of varying thickness, from 55 nm down to 12 nm. The inset shows the enlarged graphs of temperature dependence of magnetization curves for 22 nm and 12 nm thick films.
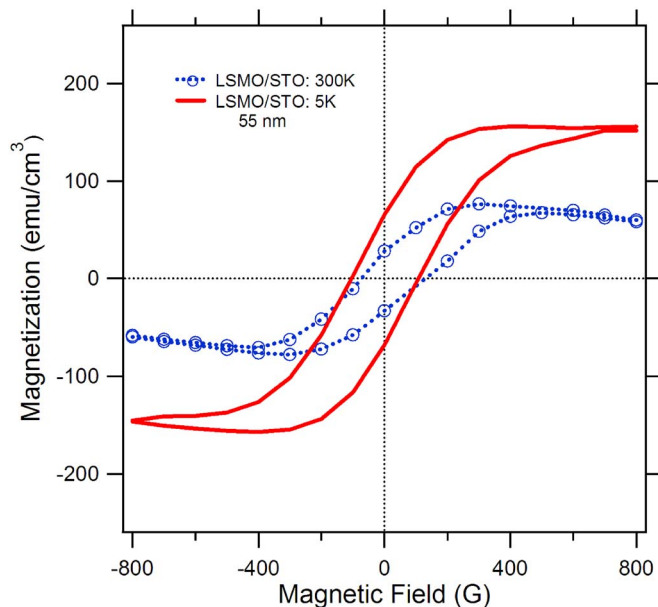
FIG. 3. (Color online) Magnetization hysteresis of 55 nm thick LSMO/STO film at 5 K and 300 K.
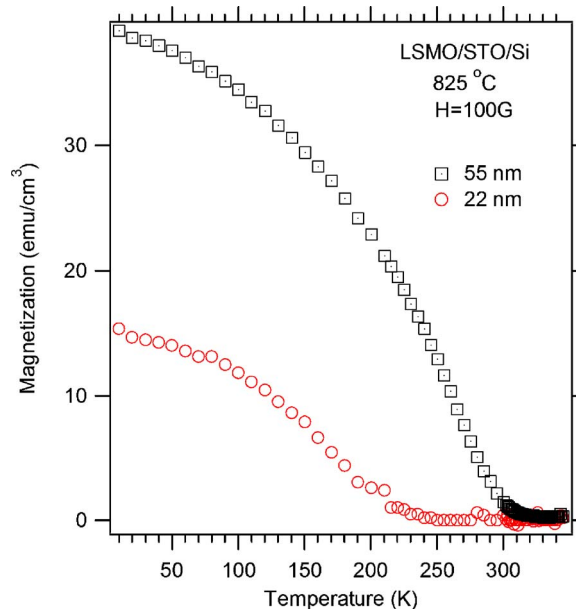

FIG. 4. (Color online) Temperature dependence of FC magnetization of LSMO/STO/Si films of varying thickness, from 55 nm down to 22 nm, grown at 825 °C.

the temperature dependence of the magnetization of the 22 nm and 12 nm films in an enlarged scale. The highest T_c was obtained at 360 K in the film at a record low thickness of 55 nm. However, as the thickness was decreased, the T_c also decreased, revealing a strong dependence of the Curie temperature on film thickness and suggesting that there is a critical thickness (t_c) at which a ferromagnetic state can no longer be maintained above room temperature in this material.

The magnetization hysteresis measurement of LSMO (55 nm)/STO film presented in Fig. 3 shows a pronounced hysteresis at 300 and 5 K, results consistent with those of previous studies of this material and verifying that LSMO/STO maintains strong ferromagnetic properties at around room temperature. However, the ferromagnetic onset transition obtained at 360 K for the LSMO/STO film of 55 nm thickness with similar composition demonstrates a record high value (360 K) compared to the previous results,[18,19] in which a 50 nm thick LSMO film on STO displays T_c=335 K, and a 300 nm thick film shows T_c=358 K. A film thickness of at least 100–200 nm is reported to retain the ferromagnetic transition temperature at 360 K, which is close to the bulk T_c of the material. The key lies in the engineering of the interface between the film and the substrate. It involves growing very high-quality single-crystalline film by tuning the growth temperature and postannealing in oxygen ambient in order to relax the strain between the film and the substrate and improve the surface morphology.

The strain relaxation of lattice mismatch between the film and the substrate at the interfaces can be explained in the following.[6] The film grows coherently, storing the biaxial strain energy below a critical thickness (t_c), above which the transition temperature of the film reaches the bulk transition temperature, such as thick films[19] and bulk samples. Above t_c, the elastic energy (due to the strain in the film, especially at the interface) in the strained film exceeds that in the core

of misfit dislocation which would be introduced at the film-substrate interface. As a result, the film is relaxed to exhibit a lattice constant similar to that of the bulk sample. Understanding and controlling the strain induced by lattice mismatch in perovskite manganites is crucial for various applications, because strains control the physical properties of the films.

The central results of the paper are the magnetic characteristics of LSMO/STO/Si films of 55 nm thickness. The temperature dependence of the FC magnetization for LSMO/STO/Si heterostructures is shown in Fig. 4 for two thicknesses: 55 nm and 22 nm. The onset of the transition temperature for the 55 nm thick film is 320 K and is decreased to ∼250 K when the thickness is decreased to 22 nm. This is a very large reduction in T_c in heterostructures compared to that of LSMO/STO films, which is related to interfacial strains and will be discussed in detail below.

For the present work, either an STO substrate or an STO template layer on Si has been chosen because of the minimal lattice mismatch (0.9%) between STO and LSMO. T_c dependence on thickness is illustrated in Fig. 5 for films of various thicknesses. We note that the film with thickness of 55 nm has been presented here for further study, except for the magnetic transition as shown in Fig. 5. T_c in the present samples is taken as the onset of magnetic transition using a magnetic field of 500 G in a field-cooled condition. It is evident that T_c decreases sharply as the thickness of the film is decreased from 55 nm to 12 nm for both films, LSMO/STO and LSMO/STO/Si. However, the decrease is larger in the case of LSMO/STO/Si as compared to LSMO directly grown on STO. The present LSMO/STO/Si films of 55 nm thickness show a T_c of about 320 K, which is close to the accepted T_c value of LSMO/STO with similar thickness.

Due to the difference in the lattice parameters of films ($a_{LSMO} \approx 3.870$ Å) and substrates ($a_{STO} \sim 3.905$ Å), the
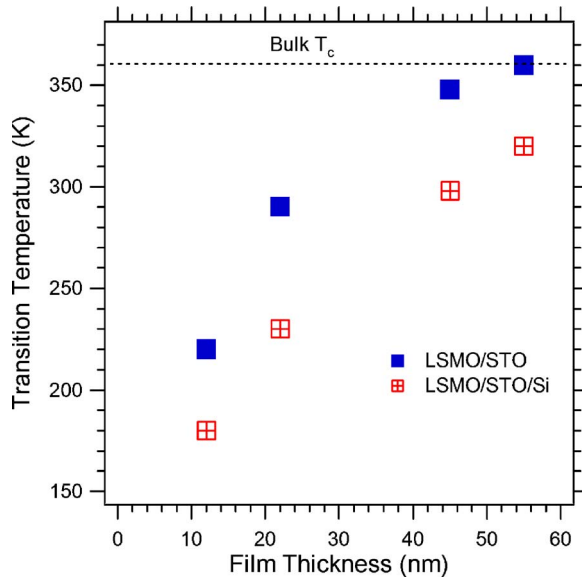
FIG. 5. (Color online) Dependence of transition temperature on film thickness for both LSMO/STO and LSMO/STO/Si films.

LSMO films are under tensile stress, which causes the films on STO to grow in a pseudomorphic mode up to a film thickness close to 55 nm. The strain is released as the critical thickness of the film reaches close to 55 nm. As the thickness of the film decreases below t_c, the relaxed top layer shows good ferromagnetic properties but the strained bottom layer in the vicinity of the interface shows degraded ferromagnetic properties. Such a scenario also explains the reduced T_c in LSMO/STO/Si films. The interface between STO and LSMO contains some tetrahedral distortions, as observed in our cross-sectional high-resolution transmission electron microscopy (HRTEM) measurements shown in Fig. 6 and described below.

The cross-sectional HRTEM shows two interface regions; LSMO/STO and STO/Si, as shown in Fig. 6(a). The STO is grown heteroepitaxially on Si and exhibits the interface layer of about 2 nm that contains disorders due to a lattice mismatch between STO and Si ($\sim$1.7%). However, beyond the 2 nm initial layer, STO maintains its crystallographic order (epitaxial). Finally, the LSMO film that is grown on STO experiences strain as well as crystallographic disorder over a few nanometers thickness, as seen in the TEM image. This eventually reduces the effective thickness of the LSMO films, as well as enhances the thickness of the strained interfacial layer in the film. This phenomenon significantly contributes to the sharp decline of T_c in LSMO/STO/Si as the thickness of the film is decreased; the oxidized interface between Si and STO especially influences the growth of STO film. The oxidized region is indicated in Fig. 6(b) by an arrow for a film in which such an oxidized Si/STO interface was observed after annealing the films. The other interface is the LSMO/STO, which shows the tetrahedral distortion as indicated in Fig. 6(b). The distorted interface can extend up to few nanometers. One of the possibilities for such distortions is the oxygen nonstoichiometry at the LSMO/STO interface. On the other hand, the surface morphology of the multilayered films is influenced by the thick-
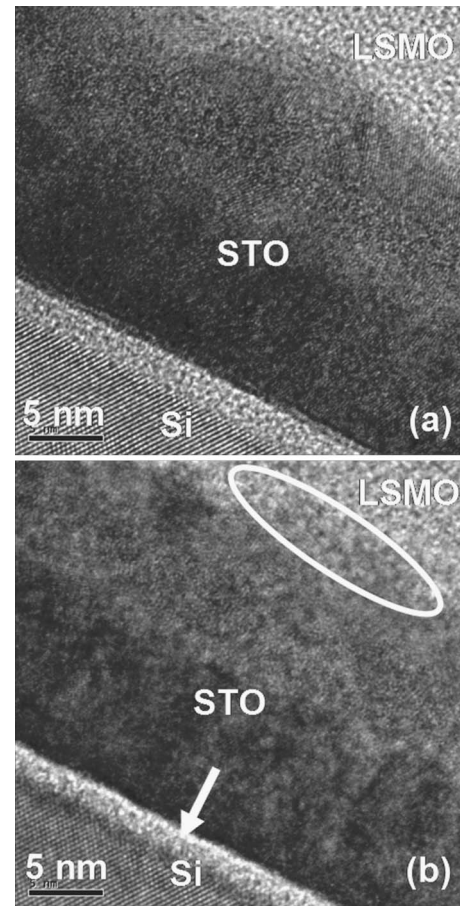

FIG. 6. TEM image of 55 nm thick LSMO/STO/Si films displaying both STO/Si and LSMO/STO interfaces (a) without oxidation between the STO/Si interface and (b) with oxidation between the STO/Si interface after annealing, and the distorted interface region between LSMO/STO, as indicated by an arrow and ellipse, respectively.

ness of the films, as shown in Fig. 7 for a thickness of (a) 22 and (b) 55 nm. It is evident that as the thickness decreases the surface shows irregular steps, although the surface roughness decreases from 2 nm to 1 nm. It is suspected that the microstrain developed at the interface between STO and LSMO has an effect on the surface morphology.

In an attempt to study the effects of growth temperature on the crystallinity and magnetic properties of the LSMO/STO/Si, 55 nm thick films of LSMO were deposited at additional growth temperatures. The surface morphology was investigated through AFM measurements in order to visualize any surface modification due to increased growth temperature. An increase in the growth temperature causes the grains at the surface of the film to coalesce, improving the overall crystallinity of the film, and there is evidence of a decrease in surface roughness due to the diffusion of the grain boundaries.

The absolute magnetization increased significantly as the film-growth temperature increased for 55 nm thick films, as shown in Fig. 8. However, no change was observed in the onset of magnetic transition. These results imply that at higher temperatures the films can transport oxygen better through diffusion, enhancing the overall crystallographic order, but varying the growth temperature does not signifi-
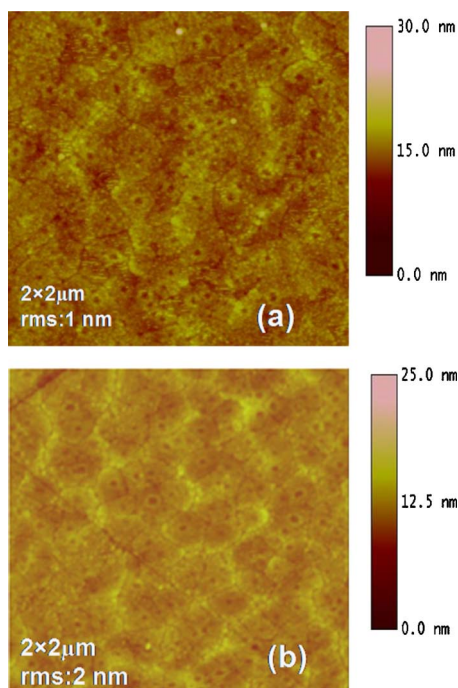
FIG. 7. (Color online) AFM images of LSMO/STO/Si (a) 22 nm and (b) 55 nm thick films.

cantly reduce the overall strain in the film—the component that was found partially responsible for the magnetic behavior in previous thickness dependence studies. In addition, other critical parameters, such as the reduction of the dead layer at the STO/Si interface due to higher growth temperature, may have a contributed to the 3 times magnetization enhancement at 10 K. However, further interface studies are necessary to confirm this.

It is well known that for LSMO tensile biaxial strain causes a reduction of T_c (Ref. 20) so that relaxation is expected to produce an increase of T_c. In order to verify this
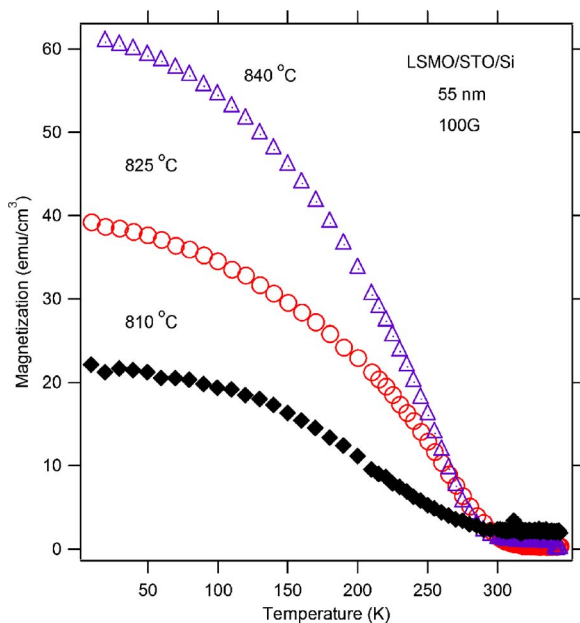

FIG. 8. (Color online) Temperature dependence of FC magnetization of 55 nm thick LSMO/STO/Si films grown at 810–840 °C.
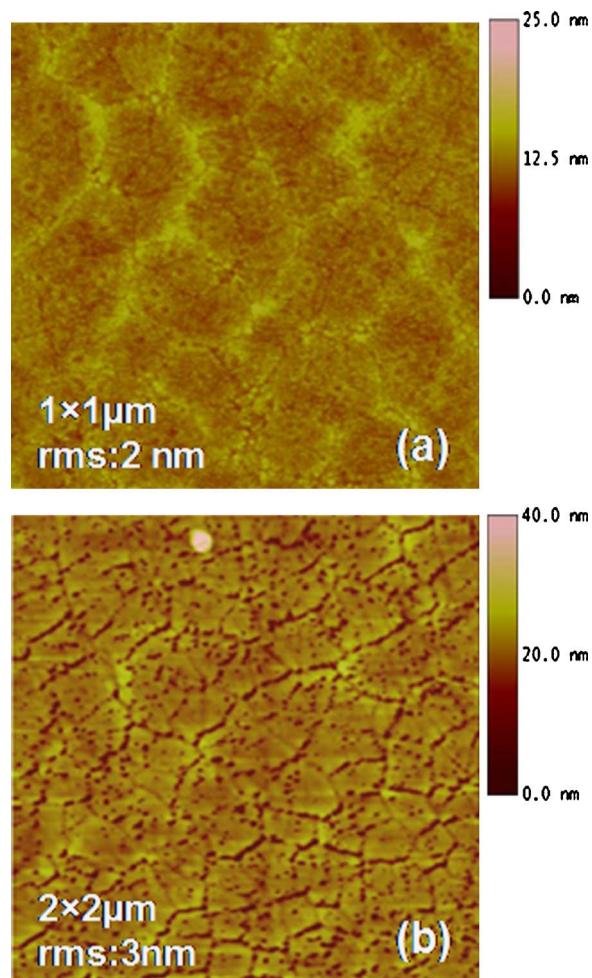

FIG. 9. (Color online) AFM images of 55 nm thick LSMO/STO/Si films (a) grown at 825 °C and (b) consequently annealed at 850 °C in oxygen for 1 h.

based on the influence of the oxygen content, we performed measurements on samples with postannealing in oxygen as done for LSMO/STO films. It has been proven that annealing in oxygen ambient at temperatures above 950 °C improves the magnetic properties of LSMO/STO due to better oxygenation and reduced crystallographic defects. As a result, one should expect to observe a similar trend in the magnetic behavior of LSMO/STO/Si as a result of annealing in oxygen. In order to test the postannealing behavior of the film, the film grown at 825 °C was annealed in oxygen at 850 °C for 1 h. The surface morphology of the film changed significantly, as shown in AFM images presented in Fig. 9 for (a) as-grown and (b) annealed films, respectively. The surface shows the coalescence of grains forming large islands with slightly increased surface roughness to 2 nm, which is mainly due to the coalescence of large domains containing nanosize grains. However, the films show large volume fractions of atomically smooth islands.

The temperature-dependent zero-field-cooled (ZFC) and FC magnetization curves are shown in Fig. 10(a) for both as-grown and annealed films. The oxygen anneal significantly enhanced magnetization, while there is hardly any enhancement in magnetic T_c. However, the field-dependent magnetization graphs [Fig. 10(b)] show a widening in the
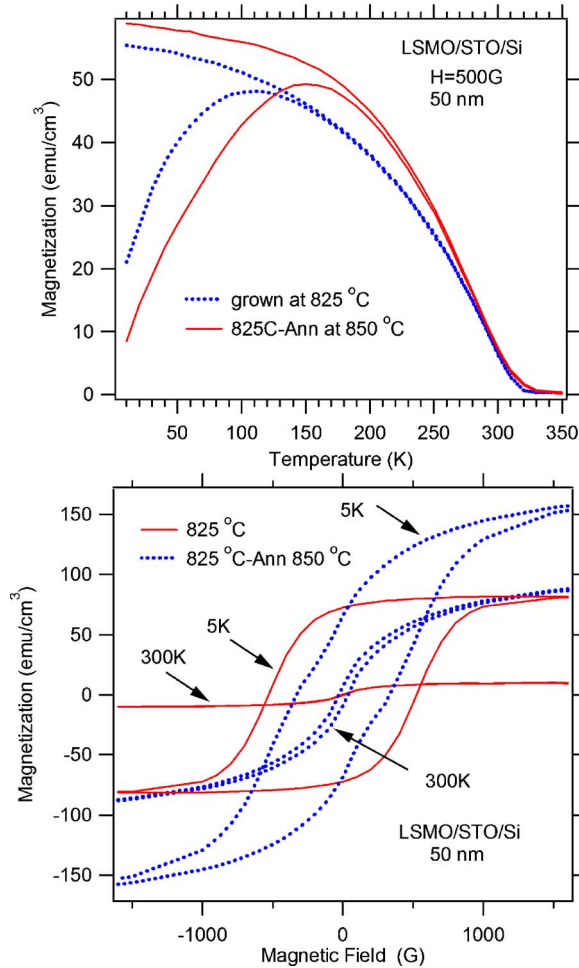
FIG. 10. (Color online) (a) Temperature dependence of FC and ZFC magnetization of 55 nm thick LSMO/STO/Si films grown at 825 °C and annealed at 840 °C. (b) Magnetization hysteresis loops of 55 nm thick LSMO/STO/Si films grown at 825 °C and annealed at 840 °C.

FIG. 11. (Color online) (a) Temperature dependence of FC and ZFC magnetization of 55 nm thick LSMO/STO/Si films at various field values.

hysteresis loop at 300 K while the film is annealed at 850 °C as compared to the as-grown film. Additionally, the saturation field increased to about 1000 G from 150 G upon annealing. This shows that annealing in oxygen at higher temperature improves the magnetic properties significantly and can make this material promising for room-temperature applications. It is suggested that although oxygenation at high temperatures increases the oxygen content in the film, enhancing the magnetization in the larger islands, the T_c is hardly affected due to the deterioration of the interfaces, as shown in Fig. 6(b), causing larger strain effects.

In order to better illustrate the magnetic ordering and homogeneity in LSMO/STO/Si, the temperature dependence of ZFC and FC magnetization curves is presented in Fig. 11. In these measurements, the sample was cooled in either zero-magnetic field (ZFC) to a desired temperature and then magnetic field was applied or field-cooled. The measurements were done while warming the sample in magnetic field for both cases. For $H=100$ G, the FC and ZFC curves separate at around 220 K with a distinct irreversibility, accompanied by a remarkable thermomagnetic hysteresis (or irreversibility) with $M_{ZFC} \neq M_{FC}$ at the irreversibility temperature T_{irr}, and $M_{FC}-M_{ZFC}$ increases as temperature decreases. How-
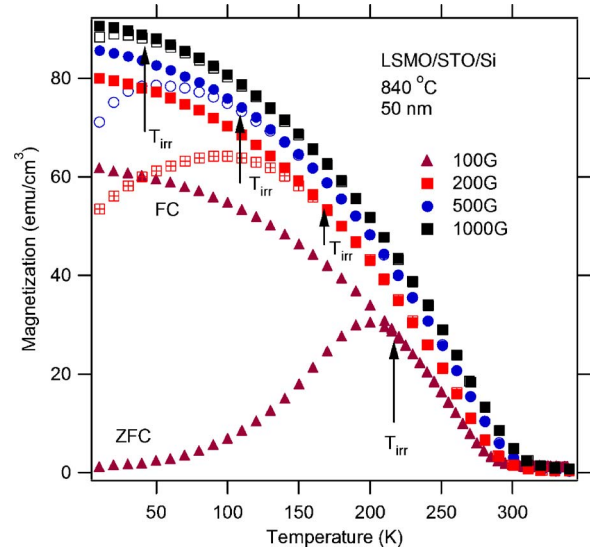
ever, for $H \geq 200$ G, $M_{FC}-M_{ZFC}$ decreases remarkably until H reaches 1000 G and T_{irr} disappears completely beyond 1000 G. This type of irreversibility in magnetization is generally indicative of antiferromagnetic (AF) ordering; however, for a simple AF no thermomagnetic hysteresis is expected. This latter effect is traditionally accepted as a hallmark of cluster-spin-glass systems with a characteristic spin-glass transition temperature T_g. This may be attributed to the presence of Mn–Mn clusters in the interface region which are antiferromagnetically coupled, and such coupling is stronger at low temperature. However, as in the case of many other manganites, the charge ordering coexists with ferromagnetism in the low-temperature phase.

We finally discuss the effects of film thickness on the transition temperature of LSMO. The ferromagnetic properties in manganites are specifically determined from two factors: (i) the double exchange of electrons between ferromagnetically coupled Mn^{3+} and Mn^{4+} ions, and (ii) the Jahn–Teller electron-phonon interaction due to lattice distortion. The strain effect on T_c and other magnetic and transport properties can be quantified to be a sum of the bulk and Jahn–Teller components. For example, T_c can be expressed[8,21] as $T_c(\varepsilon)=T_c(0)(1-\alpha\varepsilon_b-1/2\Delta\varepsilon'^2)$, where ε_b is bulk strain and $\varepsilon'=(1-a/c)$. The decrease in T_c is larger for tensile strain with $\varepsilon_b > 0$ than for compressive strain ($\varepsilon_b < 0$). As pointed out earlier,[9] the strong dependence of T_c originates from a strong interplay between the Mn e_g electron itineracy and the localizing effect of a strong electron lattice coupling. One of the strong arguments is that lifting the degeneracy of the two e_g levels due to the Jahn–Teller effect in a cubic environment by a biaxial distortion with the strain-induced biaxial distortion increases the Jahn–Teller splitting and thereby, the tendency of the electrons to become localized. Generally, a strain effect of about 1% causes a shift of T_c of about 20%. Although bulk crystals of LSMO have rhombohedral symmetry as opposed to the cubic symmetry of STO with lattice mismatch of only 0.9%, the film may not have misfit dislocation at the interface, resulting in a
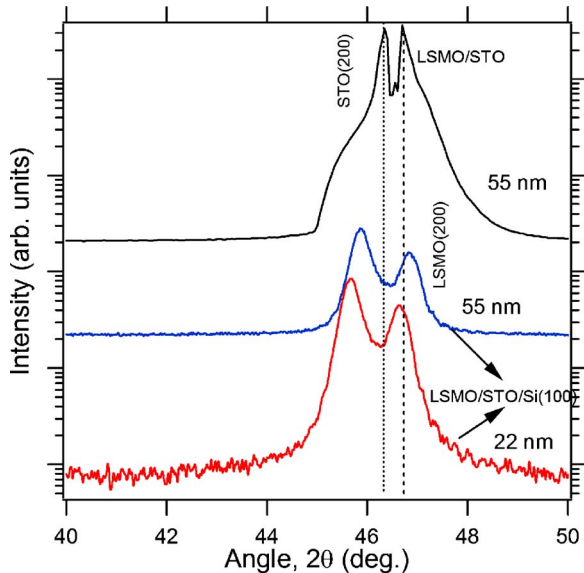
FIG. 12. (Color online) XRD patterns of LSMO/STO and LSMO/STO/Si of 55 nm and 22 nm thickness, respectively.

coherent but strained atomic arrangement. In thin films, the crystal structure of LSMO is modified to tetragonal and expanded in a lateral plane to match that of STO, in keeping with the in-plane crystal coherency at the interface. This is the fact for the present 55 nm thick LSMO/STO film under well-optimized conditions (having T_c close to the bulk sample), in contrast to 100 nm in other reports.[22] The c-axis lattice constant calculated from the X-ray diffraction (XRD) data for LSMO/STO varies from 3.86 to 3.845 Å as thickness of the film reduces from 55 to 22 nm, compared to the lattice contact of bulk LSMO (3.889 Å). This induces tensile strain in the films as thickness is reduced. However, the scenario is critical for STO-buffered Si. The LSMO film on STO-buffered Si experiences two strain effects, one incurred from the strain from Si/STO (due to the small thickness of STO) and the other from the LSMO/STO interface. The XRD patterns of LSMO/STO and LSMO/STO/Si are shown in Fig. 12 for a sample thickness of 55 nm and 22 nm in order to infer the crystallographic information. XRD confirmed that perovskite oxide heteroepitaxy on Si substrate develops with STO(001)//Si(001) and STO[100]//Si[110], as reported earlier.[23] However, although the (002) peak position for LSMO is somehow coincident with that of LSMO/STO film, the peak position for STO shifts to a lower angle, as shown in Fig. 12, illustrating variation of the lattice parameters. The c-axis lattice constant for LSMO/STO/Si varies from 3.85 to 3.84 Å, as the thickness of the film reduces from 55 to 22 nm. In view of the above, additional strain from the STO/Si layer is experienced by the LSMO films, reducing the transition temperature. Although the XRD results along with the interface defects probed by TEM give evidence for strains or interface defects which influence the physical properties of LSMO film, further structural studies are necessary to fully understand this interesting and complicated phenomenon. However, combination of these strains forms nanocrystalline grains on the surface. The reasons for such growth behavior can the explained by taking into ac-

count the Volmer–Weber type growth in which the energy relaxation takes place via the formation of 3D islands for energy minimization. The magnetic inhomogeneity observed in LSMO films of STO-buffered Si is the consequence of interface disorders which reduce T_c faster than that of LSMO on STO.

IV. CONCLUSION

We have presented the magnetic properties of LSMO films with varying thickness. The T_c of $La_{0.6}Sr_{0.4}MnO_3$ films grown directly on STO and STO-buffered Si substrates decreases sharply with decreasing film thickness. However, T_c decreases faster in films grown on STO-buffered Si substrates than those directly grown on STO. The critical thickness of 55 nm thick LSMO/STO film shows T_c at about 360 K, which is close to the bulk value, whereas T_c LSMO film on STO-buffered Si film of similar thickness is reduced to 320 K. The film surface morphology is influenced by both film thickness and postannealing. LSMO/STO/Si films, at the 55 nm thickness, were used to further investigate the effects of increasing growth temperature and postannealing in oxygen on its magnetic transition. These conditions minimally affected T_c but improved the overall magnetization of the films due to better oxygenation. However, the reduction in T_c is caused by the interface disorders due to high-temperature annealing. The thermomagnetic history effects observed in LSMO films of STO-buffered Si indicate the presence of inhomogeneity, mostly at the interface, which significantly influences the magnetic properties.

[1]A. Urushibara, Y. Moritomo, T. Arita, A. Asamitsu, G. Kido, and Y. Tokura, Phys. Rev. B **51**, 14103 (1995).
[2]J. Heremans, J. Phys. D **26**, 1149 (1993).
[3]S. Jin, M. McCormack, T. H. Tiefel, and R. Ramesh, J. Appl. Phys. **76**, 6929 (1994).
[4]J. Fontcuberta, B. Martinez, A. Seffer, S. Pinol, J. L. Garcia-Munoz, and X. Obarados, Phys. Rev. Lett. **76**, 1122 (1996).
[5]J.-Q. Wang, R. C. Barker, G.-J. Cui, T. Tamagawa, and B. L. Halperm, Appl. Phys. Lett. **71**, 3418 (1997).
[6]J. H. van der Merwe, J. Appl. Phys. **34**, 123 (1963).
[7]C. Srinitiwarawong and M. Ziese, Appl. Phys. Lett. **73**, 1140 (1998).
[8]A. J. Millis, T. Darling, and A. Migliori, J. Appl. Phys. **83**, 1588 (1998).
[9]A. J. Millis, Nature (London) **392**, 147 (1998).
[10]Y. Suzuki, H. Y. Hwang, S.-W. Cheong, and R. B. van Dover, Appl. Phys. Lett. **71**, 140 (1997).
[11]J. Aarts, S. Freisem, R. Hendrikx, and H. W. Zandbergen, Appl. Phys. Lett. **72**, 2975 (1998).
[12]M.-H. Jo, N. D. Mathur, J. E. Evetts, M. G. Blamire, M. Bibes, and J. Fontcuberta, Appl. Phys. Lett. **75**, 3689 (1999).
[13]B. Wiedenhorst, C. Ho¨fener, Y. Lu, J. Klein, L. Alff, R. Gross, B. H. Freitag, and W. Mader, Appl. Phys. Lett. **74**, 3636 (1999).
[14]B. Wiedenhorst, C. Höfener, Y. Lu, J. Klein, M. S. R. Rao, H. Freitag, W. Mader, L. Alff, and R. Gross, J. Magn. Magn. Mater. **211**, 16 (2000).
[15]M. Izumi, Y. Murakami, Y. Konishi, T. Manako, M. Kawasaki, and Y.

Tokura, Phys. Rev. B **60**, 1211 (1999).

[16]A. K. Pradhan, D. Sahu, B. K. Roul, and Y. Feng, Appl. Phys. Lett. **81**, 3597 (2002).

[17]A. K. Pradhan, S. Mohanty, K. Zhang, J. B. Dadson, E. M. Jackson, D. Hunter, R. R. Rakhimov, G. B. Loutts, J. Zhang, and D. J. Sellmyer, Appl. Phys. Lett. **86**, 012503 (2005).

[18]A. Lisauskas, J. Back, S. I. Khartsev, and A. M. Grishin, J. Appl. Phys. **89**, 6961 (2001).

[19]Yu. P. Sukhorukov, A. P. Nosova, N. N. Loshkareva, E. V. Mostovsh-chikova, A. V. Telegin, E. Favre-Nicolin, and L. Ranno, J. Appl. Phys. **97**,

103710 (2005).

[20]I. G. Deac, J. F. Mitchell, and P. Schiffer, Phys. Rev. B **63**, 172408 (2001), and references therein.

[21]H. S. Wang, E. Wertz, Y. F. Hu, Q. Li, and D. G. Schlom, J. Appl. Phys. **87**, 7409 (2000).

[22]M. Izumi, Y. Konishi, T. Nishihara, S. Hayashi, M. Sinohara, M. Ka-wasaki, and Y. Tokura, J. Appl. Phys. **73**, 2497 (1998).

[23]Z. Yu, J. Ramdani, J. A. Curless, C. D. Overgaard, J. M. Finder, R. Droo-pad, K. W. Eisenbeiser, J. A. Hallmark, W. J. Ooms, and V. S. Kaushik, J. Vac. Sci. Technol. B **18**, 2139 (2000).